Title:

On the role of phase lag in multi-appendage metachronal swimming of Euphausiids

Authors:

Mitchell P. Ford[1] and Arvind Santhanakrishnan[1,*]

Affiliations:

[1]School of Mechanical and Aerospace Engineering, Oklahoma State University, Stillwater, OK 74078, USA

Corresponding author information:

E-mail: askrish@okstate.edu

Tel: +1 4057445704

ORCID ID: 0000-0003-1800-8361

Abstract:
Metachronal paddling is a common method of drag-based biological aquatic propulsion, in which a series of swimming appendages are oscillated, with the motion of each appendage phase-shifted relative to the neighboring appendages. Ecologically and economically important Euphausiid species such as Antarctic krill (*E. superba*) swim constantly in the pelagic zone by stroking their paddling appendages (pleopods), with locomotion accounting for the bulk of their metabolic expenditure. They tailor their metachronal swimming gaits for behavioral and energetic needs by changing pleopod kinematics. The functional importance of inter-pleopod phase lag (ϕ) to metachronal swimming performance and wake structure is unknown. To examine this relation, we developed a geometrically and dynamically scaled robot ('krillbot') capable of self-propulsion. Krillbot pleopods were prescribed to mimic published kinematics of fast-forward swimming (FFW) and hovering (HOV) gaits of *E. superba*, and the Reynolds number and Strouhal number of the krillbot matched well with those calculated for freely-swimming *E. superba*. In addition to examining published kinematics with uneven ϕ between pleopod pairs, we modified *E. superba* kinematics to uniformly vary ϕ from 0% to 50% of the cycle. Swimming speed and thrust were largest for FFW with ϕ between 15%-25%, coincident with ϕ range observed in FFW gait of *E. superba*. In contrast to synchronous rowing (ϕ=0%) where distances between hinged joints of adjacent pleopods were nearly constant throughout the cycle, metachronal rowing (ϕ>0%) brought adjacent pleopods closer together and moved them farther apart. This factor minimized body position fluctuation and augmented metachronal swimming speed. Though swimming speed was lowest for HOV, a ventrally angled downward jet was generated that can assist with weight support during feeding and hydrodynamic signaling in schooling krill. In summary, our findings show that inter-appendage phase lag can drastically alter both metachronal swimming speed and the large-scale wake structure.

Keywords: Metachronal Swimming, Metachronal Paddling, Rowing, Krill Swimming, Aquatic Locomotion

1 Introduction

The coordinated rowing of multiple appendages is a common biological fluid transport mechanism used for diverse functions such as swimming in crustaceans [1-5], walking in echinoderms [6], ventilation in mayfly nymphs [7-9] and pulmonary mucus clearance in mammals [10-13]. Coordinated, sequential paddling of appendages generates a metachronal wave, such that adjacent members maintain a nearly constant phase difference [6]. Metachronal rowing is used by aquatic organisms spanning a wide range of sizes and swimming speeds, with Reynolds number (ratio of inertial forces to viscous forces) ranging from 10^{-5} for paramecia [14] to 10^{5} for escaping mantis shrimp [4]. A number of studies of metachronal swimming have investigated gait kinematics in relation to behavioral responses of a number of organisms, including paramecia [14-16], copepods [5,17-18], mysids [19], krill [20-21], mantis shrimp [4], and lobsters [22]. However, diversity of body and appendage morphologies across metachronal swimmers make it difficult to generalize how specific kinematic parameters impact swimming performance. Mechanistic studies are needed to identify unifying physical design principles underlying this successful bio-locomotion strategy. These mechanistic studies can inform evolutionary and functional biologists on the physical parameters underlying swimming performance in paddling organisms, as well as engineers working on the development of biomimetic aquatic drones.

Antarctic krill (*Euphausia superba*) are one of the most well-studied euphausiid crustaceans [1,20-21,23-26] on account of their ecological significance, with a global biomass comparable to that of humans [27]. They provide a crucial connection in oceanic food webs by grazing on smaller plankton and serving as prey for larger, commercially important animals such as fishes. Antarctic krill spend all their lives swimming in the pelagic zone, with locomotion costs accounting for nearly three-fourths of their daily metabolic expenditure [28]. This makes minimizing cost of transport essential for their survival, rather than maximizing thrust or maneuverability.

E. superba swim by periodically stroking five pairs of closely-spaced swimming appendages in an adlocomotory sequence starting from the tail to head of the animal. Pleopod pairs are phase-shifted in time relative to the neighboring pair. Geometric asymmetry is achieved in the paddling stroke with a joint located approximately halfway down the pleopod, such that the endopodite and exopodite fold up during the recovery stroke to reduce drag. The two most commonly seen swimming gaits in *E. superba* are fast-forward (FFW) and hovering (HOV) [20]. HOV gait is used by *E. superba* during feeding in laboratory settings [1,29], and in the wild [30]. Faster swimming speeds realized by FFW gait [20] can be beneficial for rapid collective behavior when schooling [31], and for predation avoidance in individual krill. These gaits exhibit differences in stroke amplitude (SA), phase lag between pleopods (ϕ), and body orientation. While we know how changing gait impacts swimming speed of *E. superba* [20], the functional importance of individual kinematic parameters (specifically SA and ϕ) on free-swimming performance remains unclear. As changes in *E. superba* gait

kinematics involve coupled changes to two or more stroke kinematic parameters, alternative approaches are necessary to identify functional roles of individual kinematic parameters. In this regard, robotic [32] and numerical [2,33-36] models can be useful to ascertain relative importance of morphological and kinematic parameters. Such studies can improve our understanding of organism-environmental interactions in terms of what factors (morphological, kinematics) render a particular species well-suited to their specific environmental niches.

Numerical studies [2,34] have shown metachronal motion to enhance thrust, while an experimental study showed that metachrony can contribute to lift [32]. Additionally, increasing Reynolds number results in the wake travelling farther downstream [32], consistent with the observation that the wake of *E. superba* can be detected several body lengths farther downstream than the wake of smaller *Euphausia pacifica* [25]. Assumptions inherent in numerical models have resulted in contradictory findings. For example, recent studies have suggested both that symmetric stroking about a vertical mean angle can [2,35] and cannot [36] generate forward motion at low Reynolds numbers. Although most modeling studies have examined tethered models of paddling propulsion [32-36], Alben et al. [2] examined swimming speed for synchronous and metachronal rowing using a simple drag coefficient model. However, they did not examine the wake structure and further neglected hydrodynamic interactions between the appendages and body. In summary, modeling efforts to date have not investigated the effects of varying stroke kinematic parameters on free-swimming performance using biologically relevant body and pleopod designs.

In this study, we developed a self-propelling paddling robot that is geometrically and dynamically similar to free-swimming *E. superba*, to examine how changing inter-pleopod phase lag (ϕ) impacts swimming speed and forward force (thrust) generation. This model, referred to as “krillbot”, is used to examine the swimming performance and the wake structure of the HOV and FFW gaits when changing ϕ. We also consider changes in body orientation angle to examine whether the larger inclination used during HOV of *E. superba* can assist with weight support by tailoring the flow field more downward. Finally, changes to instantaneous pleopod geometry are related to swimming speed to identify the physical mechanism underlying superior performance of metachronal rowing compared to synchronous rowing.

2 Methods

2.1 Geometric scaling

We developed a programmable robot to model metachronal swimming with five pairs of paddling appendages. For geometric scaling of the krillbot body, morphological measurements were acquired on a high-resolution image of an individual Antarctic krill [37] (**Figure 1A**). These measurements were used to develop simplified geometries for the krillbot body by scaling dimensions in terms of pleopod length (**Figure 1B**). Length of crustacean pleopods varies along the length of the body, but

was maintained constant in the krillbot. In krill, a joint approximately halfway down each pleopod joins the protopodite with the endopodite and exopodite. This allows the pleopod to unfold during power stroke (PS) and fold during recovery stroke (RS), creating a drag asymmetry that helps generate forward motion. Pleopod joints were modeled using 3.2 mm diameter stainless steel rods. Pleopod shape (physical model) was simplified to a rectangular protopodite on top, and endo/exopodites were combined into a trapezoidal flat plate on bottom (**Figure 1C**). The krillbot pleopods were positioned at an angle of 10º from vertical, similar to *E. superba*. This allowed the hinge to passively follow hydrodynamic forces generated by the paddling motion, as it is unknown whether crustaceans actively control their joints or allow them to passively follow the fluid.

2.2 System design and kinematics

Motion of each pair of pleopods on the krillbot was controlled by a NEMA-23 stepper motor (model ST23-4, National Instruments Corporation, Austin, TX, USA). Pleopod motion was driven by 6.4 mm (1/4 inch) timing belts that allowed the krillbot to be submerged below the fluid surface, while motors were positioned 100 mm above the fluid surface. A custom LabView (National Instruments Corporation, Austin, TX, USA) program prescribed angular positions to each stepper motor at 10 ms increments, allowing independent control of each pleopod. The LabView program communicated with the stepper motors through a National Instruments compact RIO system (cRIO-9066) connected to five stepper motor drives (SMD-7611, National Instruments Corporation) that were used to micro-step the motors to an angular resolution of 20,000 steps per revolution for precise angular control.

Experiments were performed in a 2.43 m long glass aquarium, measuring 0.65 m in width and 0.77 m in height (**Figure 2A**). The krillbot was suspended from a 1 m long low-friction air bearing (model A-108.1000, PI (Physik Instrumente) L.P., Auburn, MA, USA) that was mounted to a custom aluminum frame built around the aquarium. The air bearing allowed the krillbot to move freely along the horizontal axis, driven by the hydrodynamic forces generated from the paddling motion. Filtered air was supplied to the air bearing at 550 kPa to remove frictional effects on the suspension mechanism. The primary losses (additional to hydrodynamic drag on the body) came from fluid drag on the timing belts, and from friction on the power cables used to control the motors.

Time-variation of pleopod root angle (α in **Figure 2D**) was prescribed to a stepper motor to drive the upper part of each pleopod pair, based on individual pleopod kinematics reported for *E. superba* performing FFW and HOV gaits [20]. *E. superba* paddle their pleopods with non-uniform ϕ between adjacent pairs. Additionally, FFW and HOV kinematics of *E. superba* [20] were modified to have uniform phase lags of 0%, 15%, 25%, 35% and 50% of the cycle. For both unmodified and modified *E. superba* kinematics (for each gait), amplitude variation of α (indicative of SA) for each pleopod pair was prescribed to be identical to that of the equivalent pleopod pair of *E. superba*. For modified

E. superba kinematics, only the phase-shift between adjacent pleopods was altered to be equal (varying from 0% to 50% as noted earlier). Stroke frequency of each pleopod was identically maintained at 2.5 Hz (cycle duration, τ = 1/2.5 Hz = 0.4 s/cycle). Non-dimensionalized time t/τ was defined based on the cycle time (τ). Start time ($t = 0$ s) was defined to be the start of power stroke of the most posterior (P5) pleopod, so that t/τ = 0, 1, 2 … coincide with the start of consecutive power strokes of P5.

2.3 Dynamic scaling

The test aquarium was filled with a mixture of 85% glycerin and 15% water by volume (density, ρ=1225 kg/m^3; kinematic viscosity, ν=100 mm^2/s). This mixture allowed for matching the Reynolds number (*Re*) of flow generated by krillbot to that of freely-swimming Antarctic krill, for dynamic similarity. Pleopod *Re* was defined as:

$$Re = \frac{V_c L_c}{\nu} = \frac{(2\theta n L)L}{\nu} \quad (1)$$

where V_c and L_c are characteristic velocity and length scales, respectively. We chose pleopod length (L) as L_c and the mean pleopod tip speed for V_c. V_c is the product of stroke frequency (n) and arc length ($2\theta L$). θ represents SA of the tail-most pleopod (SA is non-uniform among pleopods [20]). Thus, *Re* is dependent on prescribed kinematics. *Re* of krill during FFW gait is about 518, while *Re* of the krillbot performing FFW kinematics is 517 (**Table 1**). For HOV, *Re* of krill is about 336, while *Re* of the krillbot performing HOV kinematics is 360 (**Table 1**). The mismatches in *Re* are due to slight differences between prescribed and achieved kinematics (**Figure 3A, Figure 3B**). However, since *Re* values are of the same order of magnitude (with <10% error), physical characteristics of the flows generated by the krillbot and by *E. superba* are expected to be comparable.

2.4 Particle image velocimetry (PIV)

Two-dimensional, two-component PIV measurements were conducted in single-frame mode at 50 frames per second using an sCMOS camera (Imager sCMOS, LaVision GmbH, Göttingen, Germany). The fluid in the tank was uniformly seeded with titanium dioxide filled polyamide particles (55 μm mean diameter). Illumination was provided using a 527 nm high-speed laser with maximum repetition rate of 1 kHz and pulse energy of 30 mJ (Photonics Industries International, Ronkonkoma, NY, USA). The laser beam was passed through collimating optics (diverging lens and converging lens) and rotated 90 degrees using a high-reflectivity mirror, after which it was passed through a cylindrical lens (-10 mm focal length) to generate a planar sheet (**Figure 2A**). The camera acquired images at 50 frames/second, with image resolution of 2560 x 2160 pixels (pixel size: 6.5 x 6.5 microns). A 50 mm constant focal length lens (Nikon Micro Nikkor, Nikon Corporation, Tokyo, Japan) was attached to the sCMOS camera with the aperture set to 2.8 for all PIV measurements. The front

of the lens was positioned 1.9 m from the mid-plane of krillbot body (lateral view), providing a field of view (FOV) of 0.63 m (length) x 0.53 m (height), with spatial resolution of 242 microns/pixel (**Figure 2A, Figure 2B**).

PIV images were acquired when the robot passed through the FOV, which was located near the end of the air bearing to ensure that the krillbot had enough time to accelerate and reach steady swimming speed. PIV data were acquired for each phase lag and gait condition at 20 degrees body angle. Velocity fields were calculated by multi-pass cross-correlation of raw images in DaVis 8.4 (LaVision GmbH, Göttingen, Germany). One pass with window size of 64x64 pixels and 2 passes with window size of 32x32 pixels, each with 50% overlap, was used for cross-correlation. Post-processing was performed to remove velocity vectors with peak ratio $Q < 1.2$, and 2D instantaneous velocity field data were exported from DaVis.

To examine rotational motion in the flow fields, out-of-plane (z) component of vorticity (ω_z) was calculated using the following equation:

$$\omega_z = \frac{\partial u}{\partial y} - \frac{\partial v}{\partial x} \tag{2}$$

where x and y represent horizontal and vertical coordinates, respectively; and u and v represent horizontal (x-component) and vertical (y-component) velocity. Wake vorticity has been tied to hydrodynamic signaling between neighboring individuals in aggregations [25].

2.5 Thrust

Forward propulsive force (thrust) was recorded using a 250 g uniaxial load cell (GSO-250, Transducer Techniques, Temecula, CA, USA). One end of the load cell was attached to the rear suspension rod between the krillbot and air bearing (**Figure 2C**), while the other end was connected to the aluminum frame via a short tether. Time-averaged thrust was calculated over one cycle. Mean and standard deviation of time-averaged thrust were taken over 20 cycles (after forces reached a steady state). Time-averaged thrust (F) was defined as:

$$F = \frac{1}{20} \sum_{n=11}^{30} \frac{1}{\tau} \int_{n\tau}^{(n+1)\tau} f(t)\, dt \tag{3}$$

where n is the cycle number, f is the time-varying thrust measured by the load cell, and τ is dimensionless time (1τ=1 cycle=0.4 s). Thrust measurements were acquired for *E. superba* FFW and HOV gait kinematics [20] and modified *E. superba* kinematics for ϕ ranging from 0% to 50%, each with body angles of 0 degrees and 20 degrees. It is important to note that these swimming gaits may not be the best-suited for accelerating from rest, as tethered organisms have been observed to greatly change their behaviors when paddling [17,38].

2.6 Swimming speed

Krillbot swimming speed was determined from high-speed videos (HSVs) acquired at 200 frames/second using a high-speed camera (Phantom Miro M110, Vision Research, Wayne, NJ, USA). The camera and attached 50 mm lens (same lens as used in PIV) was placed 2.3 m from the mid-plane of the krillbot body to give a 1.2 m long FOV, to permit recording the entire length of krillbot travel (along the 1 m long air bearing). Displacement of a fixed point (P in **Figure 2D**) was tracked in time using DLTdv7 [39] in MATLAB (The MathWorks, Inc., Natick, MA, USA). Body velocity was defined as the slope of the displacement curve. As velocity was found to vary within a cycle, we defined a mean swimming speed (V_{mean}) to characterize swimming performance:

$$V_{mean} = \frac{x(t+\tau) - x(t)}{\tau} \tag{4}$$

where $x(t)$ is displacement at time t, τ is cycle time, and $x(t+\tau)$ is displacement in one cycle after time t. This definition is the 1st order forward derivative in discrete time for one cycle. Mean swimming speed increased over the first several cycles, but achieved a constant value that was recorded as V_{mean}. Mean and standard deviations of V_{mean} were calculated across five independent trials. Representative HSVs are provided in electronic supplementary material.

2.7 Performance Metrics

The Strouhal number (St) is a commonly used dimensionless index in periodic or oscillatory flows [40] and was calculated here as:

$$St = \frac{fA}{V} \tag{5}$$

where f is the dominant frequency in the flow, while A and V are the characteristic length and velocity, respectively. Since paddling crustaceans are often found hovering, Murphy et al. [21] proposed using the maximum velocity in the wake (V_{wake}) as the characteristic velocity (as opposed to swimming speed). For the characteristic length, they used the horizontal distance traveled by the pleopod tip during PS ($A = 2L\ sin(\theta/2)$). These definitions are used here for comparison.

The advance ratio (J), a common measure of propulsive efficiency for forward motion, compares mean swimming speed to mean pleopod tip speed. In crustaceans, the advance ratio has been modified as shown below [20]:

$$J = \frac{V_{mean}}{(2\theta nL)m} \tag{6}$$

to account for the number of pleopod pairs (m).

The distance between joints (hinges) of adjacent pleopods is a representation of the time-varying geometry of the paddling system. This was compared to the variation in swimming speed within the paddling cycle. Inter-hinge distances were calculated as:

$$d_{n,n+1} = G + \frac{L}{2}\left[\sin\left(\alpha_{n+1} - \frac{\pi}{2}\right) - \sin\left(\alpha_n - \frac{\pi}{2}\right)\right] \quad (7)$$

where G is the gap between pleopods (41.9 mm), $L/2$ is the distance from the pleopod root to the hinge (38.1 mm), and α is the pleopod root angle in radians. Inter-hinge distances can be used to determine whether the body moves more quickly when pleopods are moving closer or farther from each other.

Instantaneous deviation of the body from the mean swimming speed was calculated as the difference of the actual body position in time and the estimated body position when moving at the mean velocity, as below:

$$\Delta x = x(t) - (V_{mean}t + x_{t_0}) \quad (8)$$

where Δx is the positional deviation, $x(t)$ is the position of the robot at time t, $V_{mean}t$ is the estimated position when moving at constant speed, and x_{t_0} is the displacement at some time t_0 after the krillbot has reached a periodic steady speed. By comparing Δx and d, we can examine how the motion of pleopods affects the swimming speed of the robot within the cycle. If the body velocity increases as the pleopods move quickly together, this could be due to the creation of jets of fluid being pushed away from the body. Similarly, if the robot gets a speed boost when the pleopods are moving rapidly apart, it could be due to the creation of low-pressure regions at the leading edge of the paddles during their power strokes, which would provide additional force to move the model forward relative to a model with pleopods spaced very far apart.

3 Results

3.1 Kinematics

The upper part of each pleopod pair was prescribed to match the angles that the protopodite makes with the body in *E. superba* during HOV and FFW gaits, using data in Murphy et al. [20]. The angle that the upper part of a pleopod makes with the body (i.e., pleopod root angle α), and the hinge angle (β) formed at the joint where the upper and lower parts of a pleopod meet, were tracked from HSVs using ImageJ [41]. Representative HSVs are provided in electronic supplementary material. Tracking was performed at a reduced time-resolution of 25 frames/second (every 8th frame of HSVs acquired at 200 frames/second). The results of the kinematics tracking are shown over the last full cycle of each trial (**Figure 3**), to ensure that the model had reached a steady swimming speed. Mean and standard deviations were obtained across five independent trials. For both FFW and HOV kinematics, measured pleopod root angle α (dashed lines) match well with the prescribed animal data (solid lines), meaning that our model reasonably replicated the kinematics. The hinge angles (β) are not controlled and are driven by hydrodynamic forces acting upon the pleopods. Hinge angles are qualitatively similar to the those of *E. superba* [20], with the notable exception of the

headmost/anterior pleopod (P1) during HOV. However, the hinge angles do not match as well as the pleopod root angles since they were not directly controlled.

3.2 Flow visualization

PIV measurements were conducted in order to visualize the flow field caused by the paddling motion and the vorticity in the wake. The velocity fields show direction and magnitude of the flow at discrete points in the wake. PIV calculations permit us to examine the wake structure, which is not achievable in bulk measurements such as swimming speed and thrust. PIV was performed in the mid-plane of the pleopod closest to the camera, since the pleopods of both krill and the krillbot flare out from the body, with a small gap between pleopods directly below the body. This allowed us to examine flow near the body, where it should be the fastest and strongest, since flow displaced by the pleopods must move close to the same speed as the pleopods. FFW kinematics generates a dispersed flow field (**Figure 4A-Figure 4D**), with velocity vectors pointing in various directions and a wake that is nearly one body length in width. Regions of vorticity are scattered throughout the wake when the model is performing FFW kinematics. The wake generated during HOV (**Figure 4E-Figure 4H**) is primarily in the vertical direction, with a much narrower jet than in FFW. The HOV wake is also nearly constant in time, with minimal changes throughout the stroke.

The wakes of modified FFW kinematics with uniform 0% and 15% phase lags between pleopods (**Figure 5**) are not as wide as the kinematics used by the animals with non-uniform ϕ. In this study, waveform and amplitude of the angles swept by each pleopod pair was kept the same in each case, and only phase lag between pleopods was altered. Synchronous (0% phase lag) motion generates a wake with a weaker horizontal flow component that is generally lacking in strong vortical structures away from the body (**Figure 5A-Figure 5D**). In contrast, FFW kinematics with 15% phase lag generates strong vorticity regions in the wake (**Figure 5E-Figure 5H**). This wake also has nearly constant width, rather than narrowing or spreading.

3.3 Swimming Speed

Displacement of the krillbot was tracked in time, with averages and standard deviations taken over five independent trials. Displacement for the prescribed animal kinematics is shown in **Figure 6A**. A higher slope of the displacement curve means that the krillbot moves faster. For both body angles (0° and 20°), FFW outperforms HOV by travelling the full length of the air bearing faster. Although the krillbot starts from rest and initially accelerates, it reaches a steady swimming speed after approximately 8 cycles. Using the definition of mean swimming speed from equation (4), we calculated the mean and standard deviation for each test condition (**Figure 6B**) for *E. superba* kinematics taken from Murphy et al. [20], at body angles of 0° and 20°. These are compared to mean swimming speed for modified *E. superba* kinematics with uniform phase lags of 0%, 15%, 25%,

35%, and 50% of the cycle (**Figure 6C**). We note that 50% phase lag was unachievable for FFW kinematics because the large stroke amplitude caused the paddles to collide and break. Steady swimming speed of the 15% FFW case is the same as that obtained using the FFW kinematics of *E. superba* (non-uniform ϕ). The steady swimming speed using HOV kinematics of *E. superba* (non-uniform ϕ) is similar to that obtained using modified *E. superba* HOV kinematics with uniform ϕ=25%. For both FFW and HOV, maximum swimming speed occurs in the range of 15% to 25% phase lag, which agrees with expected results based on a number of previous studies on tethered and numerical models [32,34-35].

3.4 Thrust

The krillbot allows for force measurements in a repeatable and controllable manner, which may not be possible in organismal studies. In this study, thrust was examined for different phase lags for FFW and HOV kinematics at body angles of 0 and 20 degrees. **Figure 7A** shows average thrust generated by the paddling limbs of the krillbot when tethered and performing the *E. superba* kinematics with non-uniform ϕ. FFW kinematics generate more thrust than HOV kinematics, regardless of whether the body is oriented at 0° or 20°. **Figure 7B** shows the effect of changing uniform phase lag (modified *E. superba* kinematics) on time-averaged thrust for each gait and body angle, with FFW consistently generating more thrust than HOV. HOV kinematics with a 20° body angle generates little thrust, but FFW performs similarly at 0 and 20° body orientations. The most thrust in HOV is generated when ϕ = 35-50%, while for FFW it is at ϕ =15-25%.

3.5 Comparison to swimming Euphausiids

The krillbot is approximately 11 times larger than the *E. superba* individuals recorded in Murphy et al. [20], but is geometrically similar and operates at approximately the same Reynolds number. Protopodite kinematics were prescribed to match data previously reported on freely-swimming *E. superba* [20], and matched relatively well in the krillbot (**Figure 3A-Figure 3B**). Normalized swimming speed, displacement efficiency, and advance ratio of the krillbot (**Table 1**) were lower than for two species of freely-swimming krill [20,25]. Reynolds number for the krillbot was designed to match the Reynolds numbers for Antarctic krill [20-21]. Though kinematics for this study were based on Antarctic krill, they could be easily modified to match other species as such data becomes available. The Strouhal number of the krillbot (**Table 1**) is close to the Strouhal number of freely-swimming krill, indicating that the krillbot has qualitatively similar wake structure as the krill. Although the Reynolds number and Strouhal number of the krillbot are nearly the same as for the animals, lower advance ratios are observed for the krillbot despite identical kinematics as *E. superba*. This suggests that the relatively lower swimming performance of the krillbot is due primarily to added drag from the assembly (cabling resistance, drag generated by krillbot suspension), and possibly also due

to restriction of one-dimensional travel. Additionally, the simplified geometries of the rigid krillbot pleopods could contribute to lower thrust coefficients in the krillbot than in live animals.

4 Discussion

Albeit several studies of metachronal propulsion have been performed in freely-swimming crustaceans [4,19,21] and using numerical [2,33-35] and robotic models [32,36], the effects of varying individual stroke kinematic parameters on free-swimming performance are unclear. We examined free-swimming performance as a function of inter-pleopod phase delay (ϕ) using a self-propelled biomimetic krill robot. Krillbot pleopods were programmed to move using previously published fast-forward swimming (FFW) and hovering (HOV) gait kinematics of freely-swimming Antarctic krill, *E. superba* [20]. Additionally, ϕ was varied from 0% of the stroke period to a maximum of 35% (FFW) or 50% (HOV). Swimming performance was assessed using free-swimming speed and tethered thrust force. Regardless of phase lag, metachronal motion of pleopods (non-zero ϕ) resulted in increasing swimming speed and thrust compared to synchronous paddling (ϕ=0%). Flow visualization showed dramatic differences between the two gaits. The angled jet generated by HOV gait can enable downward momentum transfer for animal weight support needed during *E. superba* feeding. Further, the coherent wake structure generated by HOV gait can potentially assist in hydrodynamic signaling between neighboring krill. By contrast, the wider and stronger wake generated by FFW gait can enable fast maneuvers needed for predator avoidance. To the best of the authors' awareness, this is the first study to report: 1) thrust generated by FFW and HOV gaits of *E. superba*; 2) effect of varying ϕ on free-swimming performance; 3) flow generated by FFW gait of *E. superba*; and 4) fluid dynamic mechanism underlying thrust augmentation by metachronal rowing (i.e., non-zero ϕ).

Despite simplifications in the krillbot pleopod design, including the lack of 'lobed' structure (with endopodite and exopodite), rigid structure, and the absence of setae, our robotic model characteristics compare well with those of free-swimming *E. superba* and *E. pacifica* (**Table 1**). The krillbot is able to reasonably mimic pleopod motion of two distinct *E. superba* swimming gaits (FFW and HOV). Strouhal number of the krillbot matches that of *E. superba* when the geometry, Reynolds number, and kinematics are the same. However, losses in the system (resistance offered by cabling, drag generated by suspension system) inevitably result in lower displacement efficiency in the krillbot than in live crustaceans. The flow generated by the krillbot in HOV gait was similar to that reported in hovering *E. superba* [21]. The jet-like flow observed in FFW gait of the krillbot also resembled wake flow generated by freely-swimming *E. superba* reported by Catton et al. (gait not identified) [25]. Overall, these comparisons provide validity in using the krillbot for biologically

relevant mechanistic studies as in this paper, toward identifying specific roles of individual stroke kinematic parameters on free-swimming performance.

FFW gait with phase lags (ϕ) ranging between 15% to 25%, similar to the range of ϕ reported in FFW gait of freely-swimming *E. superba*, were found to provide highest thrust and swimming speed. This is also within the range of ϕ where highest average volumetric flux was obtained in previous computational modeling studies of tethered metachronal propulsion [34,35], as well as within the range of ϕ where largest fluid momentum was observed in a previous study using a tethered metachronal robotic model [32]. Zhang et al. [34] argued that geometries generated by adjacent pleopods stroking at ϕ=25% could help in entrapping more volume of fluid in the inter-pleopod gap during PS and less volume of fluid during RS. However, they did not examine free-swimming performance with their modeling approach.

To examine the fluid dynamic mechanism augmenting krillbot thrust for ϕ >0%, we characterized the distance between hinges of adjacent pleopods (**Figure 8A**-**Figure 8B**). For synchronous pleopod motion (ϕ=0%), the distance between hinges is nearly constant (≈42 mm, **Figure 8A**). However, when phase lag is increased, the pleopods move relative to each other, resulting in periodic fluctuations in the hinge distance (**Figure 8B**). By comparing the hinge distances to the displacement, we were able to determine that in general, the krillbot slows down when two adjacent pleopods move towards each other and speeds up when two adjacent pleopods move apart from each other (**Figure 8C**-**Figure 8D**). When two pleopods move towards each other, high pressure is to be expected in the space between the pleopods. Such a high pressure region would generate a jet emanating ventrally down from the gap between pleopods. Likewise, when two pleopods move apart from each other, a low-pressure region is expected in the inter-pleopod gap. The low-pressure region provides a suction on the leading edge of the more posterior pleopod. This is consistent with *in vivo* observations on other species, suggesting that the pressure gradient developed in the inter-pleopod gap due to the periodic motion of the pleopods (dictated by the phase lag) plays a significant role in forward motion [15,19]. Additionally, krill and other freely-swimming crustaceans typically have jointed pleopods that are able to fold during the recovery stroke (RS) and unfold during the power stroke (PS). This provides a large surface area during PS that increases thrust, and a much smaller surface area during RS that helps to minimize drag (i.e., negative thrust).

In addition to swimming performance changing with the swimming gait, the wake structure changes as well. While the wake of the FFW motion forms a large "wall" of fluid moving in the opposite direction of the krillbot, the wake generated by the HOV motion forms a clearly-defined jet moving ventrally and towards the tail of the model. This ventrally angled jet generated by HOV gait can enable downward momentum transfer for weight support needed during *E. superba* feeding [21]. In addition, this well-defined jet could be useful in contributing to any of the variety of proposed

hypotheses for signaling and energy-saving in schooling krill [25,26]. It is believed that the regular structure of these schools helps krill communicate with each other, and that it allows them to save energy which helps their survival. The regular structure of the HOV wake, as opposed to the more-dispersed wake of the FFW gait, could contribute to this ability of the hovering krill to form these aggregates. By contrast, the wider and stronger wake jet generated by FFW gait can enable fast maneuvers needed for predator avoidance among individuals and rapid collective behavior exhibited by schooling krill [31].

5 Conclusions

Using a self-propelling krill robot, we show that the phase lag range (ϕ=15%-25%) used in FFW and HOV gaits of freely-swimming Antarctic krill (*E. superba*) is well-suited for achieving peak swimming performance (FFW), for downward transfer of momentum, and for hydrodynamic signaling (HOV). Variation of inter-pleopod phase lag in metachronal swimming directly affects steady swimming speed during self-propulsion. Swimming speed increases when closely spaced limbs move away from each other, and decreases when they move closer together. Collectively, these findings illustrate the foremost importance of phase lag in free-swimming performance of coordinated rowing with multiple appendages.

Ethics. This article does not present research with ethical considerations.

Data Accessibility Statement. Electronic supplementary material consisting of representative high-speed videos of krillbot motion, and numerical data used in figures 3, 6, 7 and 8 are available within Figshare: https://figshare.com/s/030703a893e43ef4cfa8 [42]. (Note: this is a private link for the review process and will be made public with a DOI if/when manuscript is accepted).

Authors' Contributions. M.P.F. and A.S. conceived of and designed the study. M.P.F. acquired experimental data. M.P.F. and A.S. analyzed the data, drafted and critically revised the manuscript. All authors gave final approval for publication and agree to be held accountable for the work performed therein.

Competing Interests. We declare we have no competing interests.

Acknowledgements. We would like to thank Tyler Blackshare for his assistance with tracking kinematics of krillbot pleopod motion.

Funding. This work was supported by the National Science Foundation (grant number CBET 1706762 to A.S.).

References

1. Kils U. 1981 Swimming behaviour, swimming performance and energy balance of Antarctic krill *Euphausia superba*. BIOMASS Sci. Ser. 3, 1–21.

2. Alben S, Spears K, Garth S, Murphy D, Yen J 2010 Coordination of multiple appendages in drag-based swimming J. R. Soc. Interface 7, 1545–1557

3. Lenz P H, Takagi D, Hartline D K 2015 Choreographed swimming of copepod nauplii J. R. Soc. Interface 12

4. Campos E O, Vilhena D, Caldwell R L 2012 Pleopod rowing is used to achieve high forward swimming speeds during the escape response of *Odontodactylus havanensis* (Stomatopoda) J. Crustacean Biol. 32, 171–179

5. Van Duren L A, Videler J J 2003 Escape from viscosity: The kinematics and hydrodynamics of copepod foraging and escape swimming J. Exp. Biol. 206, 269–279

6. Sleigh, M A, & Barlow, D I 1980 Metachronism and control of locomotion in animals with many propulsive structures. In: Elder, H Y and Trueman, E R , (ed) *Aspects of Animal Movement,* Cambridge University Press, Cambridge, pp 49-70

7. Larson M, Kiger K T, Abdelaziz K, Balaras E 2014 Effect of metachronal phasing on the pumping efficiency of oscillating plate arrays Exp. Fluids 55

8. Sensenig A T, Kiger K T, Shultz J W 2009 The rowing-to-flapping transition: Ontogenetic changes in gill-plate kinematics in the nymphal mayfly *Centroptilum triangulifer* (Ephemeroptera, Baetidae) Biol. J. Linn. Soc. 98, 540–555

9. Sensenig A T, Kiger K T, Shultz J W 2010 Hydrodynamic pumping by serial gill arrays in the mayfly nymph *Centroptilum triangulifer* J. Exp. Biol. 213, 3319–3331

10. Sleigh M A, Blake J R, Liron N 1988 The propulsion of mucus by cilia Am. Rev. Respir. Dis. 137, 726–741

11. Wong L B, Miller I F, Yeates D B 1993 Nature of the mammalian ciliary metachronal wave J. Appl. Physiol. 75, 458–467

12. Elgeti J, Gompper G 2013 Emergence of metachronal waves in cilia arrays Proc. Natl. Acad. Sci. U. S. A. 110, 4470–4475

13. Chateau S, Favier J, Poncet S, D'Ortona U 2019 Why antiplectic metachronal cilia waves are optimal to transport bronchial mucus Phys. Rev. E 100, 42405

14. Bandyopadhyay P R, Hansen J C 2013 Breakup and then makeup: A predictive model of how cilia self-regulate hardness for posture control Sci. Rep. 3, 1–10

15. Jana S, Um S H, Jung S 2012 Paramecium swimming in Capillary Tube Phys. Fluids 041901

16. Funfak A, Fisch C, Abdel Motaal H T, Diener J, Combettes L, Baroud C N, Dupuis-Williams P 2015 Paramecium swimming and ciliary beating patterns: A study on four RNA interference mutations Integr. Biol. (United Kingdom) 7, 90–100

17. Catton K B, Webster D R, Brown J, Yen J 2007 Quantitative analysis of tethered and free-swimming copepodid flow fields J. Exp. Biol. 210, 299-310

18. Jiang H, Kiørboe T 2011 The fluid dynamics of swimming by jumping in copepods J. R. Soc. Interface 8, 1090–1103

19. Schabes M and Hamner W 1992 Mysid locomotion and feeding: kinematics and water-flow patterns of *Antarctomysis* sp ., *Acanthomysis sculpta*, and *Neomysis rayii* J. Crustacean Biol. 12, 1–10

20. Murphy D W, Webster D R, Kawaguchi S, King R, Yen J 2011 Metachronal swimming in Antarctic krill: Gait kinematics and system design Mar. Biol. 158, 2541–2554

21. Murphy D W, Webster D R, Yen J 2013 The hydrodynamics of hovering in Antarctic krill Limnol. Oceanogr. Fluids Environ. 3, 240–255

22. Lim J L, DeMont M E 2009 Kinematics, hydrodynamics and force production of pleopods suggest jet-assisted walking in the American lobster (*Homarus americanus*) J. Exp. Biol. 212, 2731–2745

23. Wiese K, Ebina Y 1995 The propulsion jet of *Euphausia superba* (Antarctic Krill) as a potential communication signal among conspecifics J. Mar. Biol. Assoc. United Kingdom 75, 43–54

24. Zhou M, Dorland R D 2004 Aggregation and vertical migration behavior of *Euphausia superba* Deep. Res. Part II Top. Stud. Oceanogr. 51, 2119–2137

25. Catton K B, Webster D R, Kawaguchi S, Yen J 2011 The hydrodynamic disturbances of two species of krill: Implications for aggregation structure J. Exp. Biol. 214, 1845–1856

26. Murphy D W, Olsen D, Kanagawa M, King R, Kawaguchi S, Osborn J, Webster D R, Yen J 2019 The three dimensional spatial structure of Antarctic krill schools in the laboratory Sci. Rep. 9, 1–12

27. Atkinson A, Siegel V, Pakhomov E A, Jessopp M J, Loeb V 2009 A re-appraisal of the total biomass and annual production of Antarctic krill Deep. Res. Part I Oceanogr. Res. Pap. 56, 727–740

28Swadling K M, Ritz D A, Nicol S, Osborn J E, Gurney L J 2005 Respiration rate and cost of swimming for Antarctic krill, *Euphausia superba*, in large groups in the laboratory Mar. Biol. 146, 1169–1175

29. Endo Y 1993 Orientation of Antarctic Krill in an Aquarium Nippon Suisan Gakkaishi 59, 465–468

30. Marschall H P 1988 The overwintering strategy of Antarctic krill under the pack-ice of the Weddell Sea Polar Biol. 9, 129–135

31. Hamner W M 1984 Aspects of schooling in *Euphausia superba* J. Crustacean Biol. 4, 67–74

32. Ford M P, Lai H K, Samaee M, Santhanakrishnan A 2019 Hydrodynamics of metachronal paddling: effects of varying Reynolds number and phase lag R. Soc. Open Sci. 6, 191387

33. Takagi D 2015 Swimming with stiff legs at low Reynolds number Phys. Rev. E 92, 023020

34. Zhang C, Guy R D, Mulloney B, Zhang Q, Lewis T J 2014 Neural mechanism of optimal limb coordination in crustacean swimming Proc. Natl. Acad. Sci. U. S. A. 111, 13840–13845

35. Granzier-Nakajima S, Guy R D, Zhang-Molina C 2020 A Numerical Study of Metachronal Propulsion at Low to Intermediate Reynolds Numbers Fluids 5, 86

36. Hayashi R, Takagi D 2020 Metachronal swimming with rigid arms near boundaries Fluids 5, 24

37. Kils, U 2011 "Antarctic krill (Euphausia superba).jpg", used under Creative Commons Attribution-Share Alike 3.0 Unported license / Background removed and dimensional annotations added

38. Yen J, Brown J, Webster D R 2003 Analysis of the flow field of the krill, *Euphausia pacifica* Mar. Freshw. Behav. Physiol. 36, 307–319

39. Hedrick T L 2008 Software techniques for two- and three-dimensional kinematic measurements of biological and biomimetic systems Bioinspiration and Biomimetics 3

40. Taylor G K, Nudds R L, Thomas A L R 2003 Flying and swimming animals cruise at a Strouhal number tuned for high power efficiency Nature 425, 705–707

41. Schneider C A, Rasband W S, Eliceiri K W 2012 NIH Image to ImageJ: 25 years of image analysis Nat. Methods 9, 671–675

42. Ford M, Santhanakrishnan A 2020 Data from: On the role of phase lag in multi-appendage metachronal swimming of Euphausiids. Figshare private link (will be made public with a DOI if/when manuscript is accepted): https://figshare.com/s/030703a893e43ef4cfa8.

Tables

Metric	Swimming mode	*E. pacifica*	*E. superba*	Krillbot
Body Length (cm)	N/A	2.7	3.8-5.5	46.4
Limb Length (cm)	N/A	0.25	0.65	7.62
Number of Pleopod Pairs	N/A	5	5	5
Maximum Stroke Amplitude (degrees)	HOV	—	76	71
	FFW	111	105	102
Pleopod Beat Frequency (Hz)	HOV	5.6	3	2.5
	FFW	10.9	3	2.5
Swimming Speed (cm/s)	HOV	2.6	1	4.9
	FFW	15.5	7.7	15.3
Normalized speed (BL/s)	HOV	1	0.26	0.1
	FFW	4.84	1.5	0.33
Displacement Efficiency (BL/stroke)	HOV	0.46	0.09	0.04
	FFW	0.44	0.46	0.13
Advance ratio	HOV	0.096*	0.039	0.02
	FFW	0.29	0.19	0.045
Reynolds Number	HOV	135*	336	360
	FFW	264	518	517
Strouhal Number	HOV	—	0.37	0.44
	FFW	—	0.38	0.45

* = stroke amplitude for FFW *E. pacifica* used for calculations

Table 1. Metrics used to compare the krillbot swimming performance to the swimming performance of live *Euphausia pacifica* and *Euphausia superba*. The kinematics used in this study came from *E. superba* [20]. Data for *E. pacifica* and *E. superba* obtained from [20,25]. The krillbot is approximately 11 times larger than *E. superba*, but swims at approximately the same Reynolds number. Displacement efficiency, advance ratio, and Strouhal number allow for direct comparison to the live animal swimming performance. Displacement efficiency is lower in the krillbot than in krill, and the lower displacement efficiency leads to a lower advance ratio. However, as both the Strouhal number and Reynolds number are similar, the krillbot is dynamically similar to the freely-swimming krill for hovering (HOV) and fast forward swimming (FFW) gaits.

Figure captions

Figure 1. Geometric scaling of krill and krillbot design. (A) Antarctic krill (*Euphausia superba*) with lengths nondimensionalized relative to the pleopod length (L). Image of *E. superba* adapted and edited from Kils [37]. (B) Dimensions of the robotic paddling model ("krillbot") specified in mm. The body length of the robotic model is approximately 8-11 times the body length of adult *E. superba*, and is geometrically similar. (C) Front view of a pair of krillbot pleopods (physical models). Krillbot pleopod geometry is simplified to that of *E. superba*, such that all model pleopods are of the same length and a hinge is located halfway down the length of each model pleopod. Below the hinge point, model pleopod geometry is simplified to a trapezoidal flat plate with area geometrically similar to that of *E. superba* pleopods. Rigid, solid pleopods are used on the krillbot as compared to feather-like pleopods of *E. superba* with long setae at the fringes.

Figure 2. Experimental apparatus. (A) Camera view used in PIV data acquisition. A laser sheet from below is used to illuminate seeding particles added in the tank. The krillbot is suspended from a low-friction linear air bearing that is 1 m long. The krillbot can move forward or backward using self-generated propulsive force with minimal resistance from the suspension assembly. (B) Top view of the PIV setup, showing the laser plane located at the centerline axis of the model pleopod closest to the camera. Model pleopods were made using clear acrylic to allow laser light to pass through, necessary to resolve flow velocities near the body. (C) Schematic of the experimental setup used for force measurements. A uniaxial load cell attached to the krillbot suspension was used to measure forward (thrust) force generated by the krillbot when model pleopods were in motion. (D) Close-up image of the krillbot from a representative high-speed video used to quantify swimming speed. The position of the mounting screw (labeled P) near the head (H) of the model was tracked in each frame of video recordings, and used to determine the displacement of the krillbot in time for the determination of swimming speed. Pleopods are labeled with increasing numerical values from anterior (P1) to posterior (P5) located closest to the tail (T). Time-variation of pleopod root angle (α) was prescribed. Hinged joints were located approximately halfway along the vertical length of each pleopod. These joints allowed for pleopods to passively fold during recovery stroke (RS) and unfold in power stroke (PS). Both α and hinge angle (β) were tracked in time from high-speed videos.

Figure 3. Pleopod kinematics of Antarctic krill from Murphy et al. [20] and krillbot. (A) Pleopod root angle (α) versus time for fast-forward (FFW) kinematics for the last full cycle (t = instantaneous cycle time; τ = cycle duration = 0.4 s). Krillbot pleopod kinematics were tracked across 5 independent trials. Solid lines represent the prescribed motion, obtained from *E. superba* [20] and dashed lines represent the mean kinematics achieved by the krillbot (shading represents $\pm$1 standard deviation).

(B) α versus time for hovering (HOV) kinematics. (C) Hinge angle β versus time for FFW kinematics. Unlike α, hinge angle β was not actively controlled. The lower portion of the pleopod was allowed to rotate freely about its hinge point, following the hydrodynamic forces generated by the paddling motion. (D) β versus time for HOV kinematics. Despite the use of passive hinges with highly simplified geometries, hinge angle β for the model agrees reasonably well with β versus time observed in freely-swimming *E. superba*. Representative high-speed videos used for tracking are provided in electronic supplementary material.

Figure 4. Out-of-plane vorticity contours overlaid with velocity fields generated by krillbot prescribed to move using FFW (A-D), and HOV (E-H) kinematics of *E. superba* [20]. Time points are defined based on the position of the tail-most pleopod (P5 in **Figure 2D**). (A & E) Start of PS. (B & F) Middle of PS. (C & G) End of PS, which coincides with the start of RS. (D & H) Middle of RS. The wake generated by FFW kinematics (A-D) is seen to be quite dispersive of vorticity relative to the wake generated by HOV kinematics (E-H). The nearly steady, relatively coherent jet generated by the hovering kinematics could contribute to hydrodynamic signaling that allows larger species of krill such as *E. superba* to form coordinated groups.

Figure 5. Out-of-plane vorticity contours overlaid with velocity fields generated by krillbot when prescribed to move using modified FFW kinematics of *E. superba* such that phase lag between adjacent pleopods were equal. (A-D) show synchronous pleopod motion, while (E-H) show metachronal motion with uniform 15% phase lag. Time points are defined based on the position of the tail-most pleopod (P5 in **Figure 2D**). (A & E) Start of PS. (B & F) Middle of PS. (C & G) End of PS / start of RS. (D & H) Middle of RS. Synchronous motion (A-D) exhibits a wavy, periodic wake structure, while the metachronal motion exhibits a more continuous wake.

Figure 6. Self-propulsion characteristics of the krillbot. (A) Krillbot displacement versus non-dimensional time (t/τ) for prescribed non-uniform/unequal ϕ (*E. superba*) kinematics with different gaits and phase lags. (B) Steady swimming speed for the conditions shown in (A). The slope of the time-varying displacement curve in (A) approaches a steady value, which is the speed shown in (B). (C) Steady swimming speed for varying phase lag and gait for modified *E. superba* kinematics with uniform ϕ. Changing ϕ results in changing the forward swimming speed. For both FFW and HOV, uniform 15% phase lag shows nearly equal swimming speed (in C) as non-uniform phase lag (in B). (D) Advance ratio for varying gait, body angle, and phase lag, calculated using equation (6). Advance ratio is a performance measure which compares the forward body velocity to the velocity of

the propulsive appendages. Higher advance ratio is generally regarded as a measure of better propulsive performance.

Figure 7. Time-averaged thrust (forward force) generated for varying ϕ and body angle. The krillbot was tethered using a uniaxial load cell (illustrated in **Figure 2C**) which was used to measure the forward propulsive force generated by the pleopod paddling. Regardless of phase lag and body angle tested, FFW kinematics (both unequal ϕ as in *E. superba* and modified *E. superba* FFW kinematics with uniform ϕ) generated more forward force than HOV kinematics. For FFW, non-uniform phase lag (in A) was found to generate nearly the same thrust as uniform (15%) phase lag (in B).

Figure 8. Inter-hinge distances and body position deviation when krillbot was prescribed to move with FFW kinematics modified from *E. superba* FFW kinematics, such that ϕ was uniform between pleopod pairs. Synchronous rowing with ϕ=0% is shown in left column and metachronal rowing with ϕ=15% is shown in right column. Instantaneous values of body position deviation (Δx) were calculated as the difference between measured position and estimated position when moving at steady swimming speed, using equation (8). $t/\tau = 0$ refers to the start of power stroke of the last full cycle in each case ($\phi = 0\%$ and $\phi = 15\%$). Inter-hinge distance (from equation (7)) between pleopod pairs for FFW kinematics was nearly constant at 0% phase lag (shown in A) as compared to periodic fluctuations for 15% phase lag (shown in B). Pleopods move farther apart when inter-hinge distance is increasing, and come closer together when this distance is decreasing. Δx was larger for ϕ=0% (shown in C) as compared to ϕ=15%-35% (shown in D). Time-variation of Δx for ϕ=0% are dominated by low (1x per cycle) frequency.

Figure 1

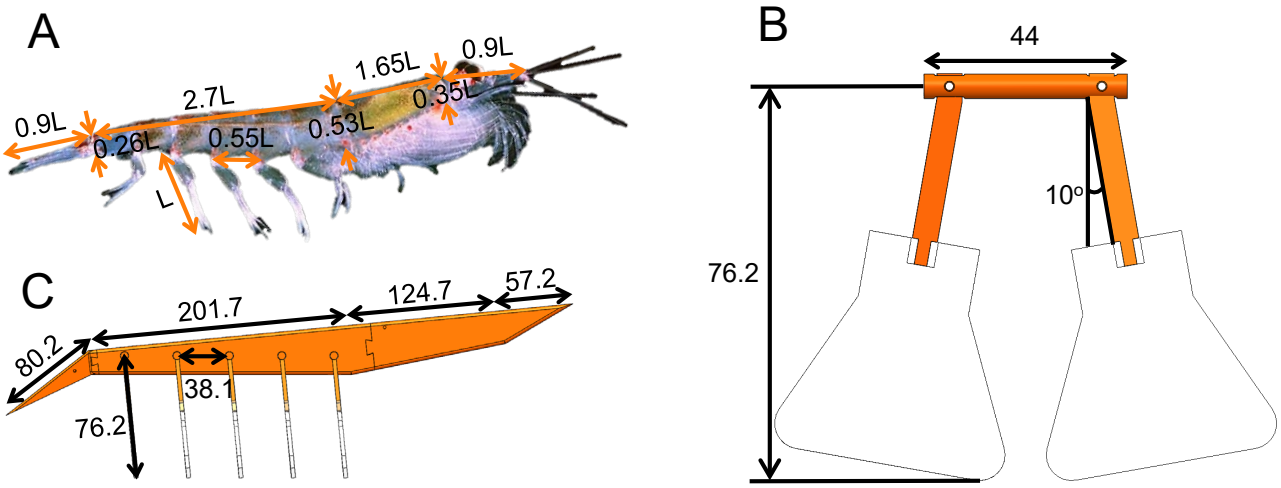
A
0.9L
0.26L
2.7L
0.55L
0.53L
1.65L
0.35L
0.9L
L
B
44
10°
76.2
C
80.2
201.7
124.7
57.2
38.1
76.2

Figure 2

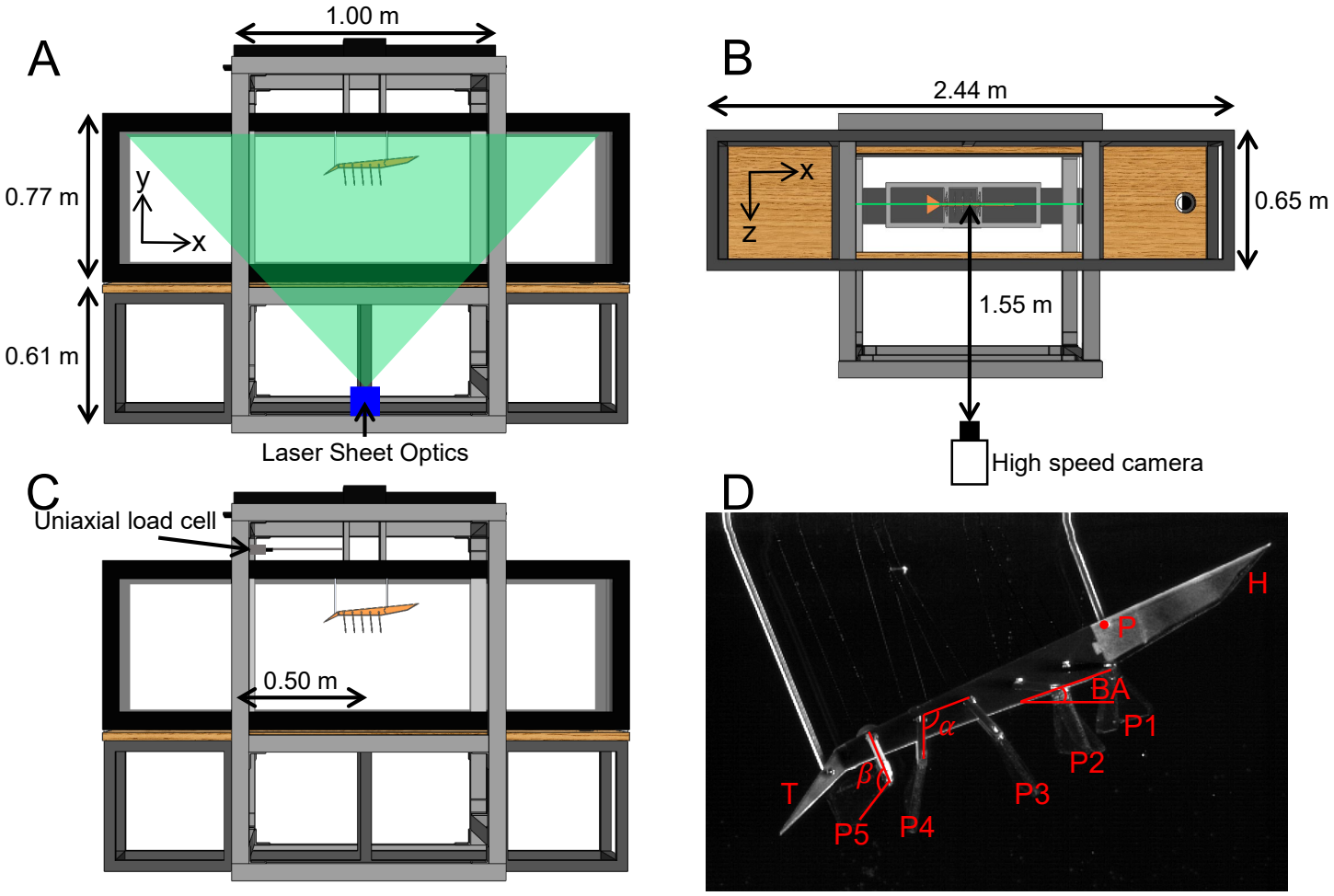
A
1.00 m
0.77 m
0.61 m
y
x
Laser Sheet Optics
B
2.44 m
0.65 m
x
z
1.55 m
High speed camera
C
Uniaxial load cell
0.50 m
D
H
P
BA
P1
P2
P3
P4
P5
T
α
β

Figure 3

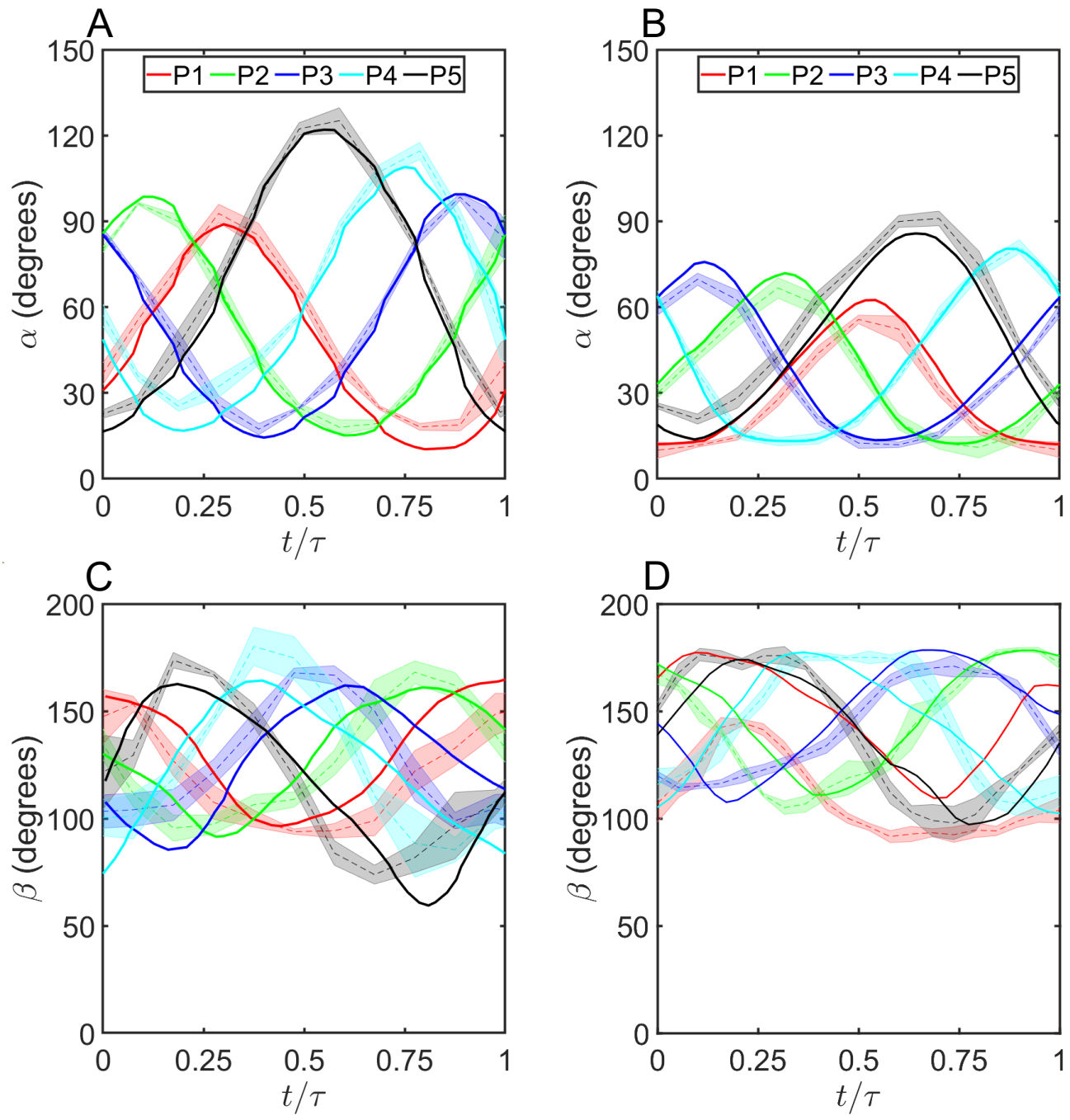
A
B
C
D
P1
P2
P3
P4
P5
α (degrees)
β (degrees)
t/τ
0
30
60
90
120
150
50
100
200
0.25
0.5
0.75
1

Figure 4

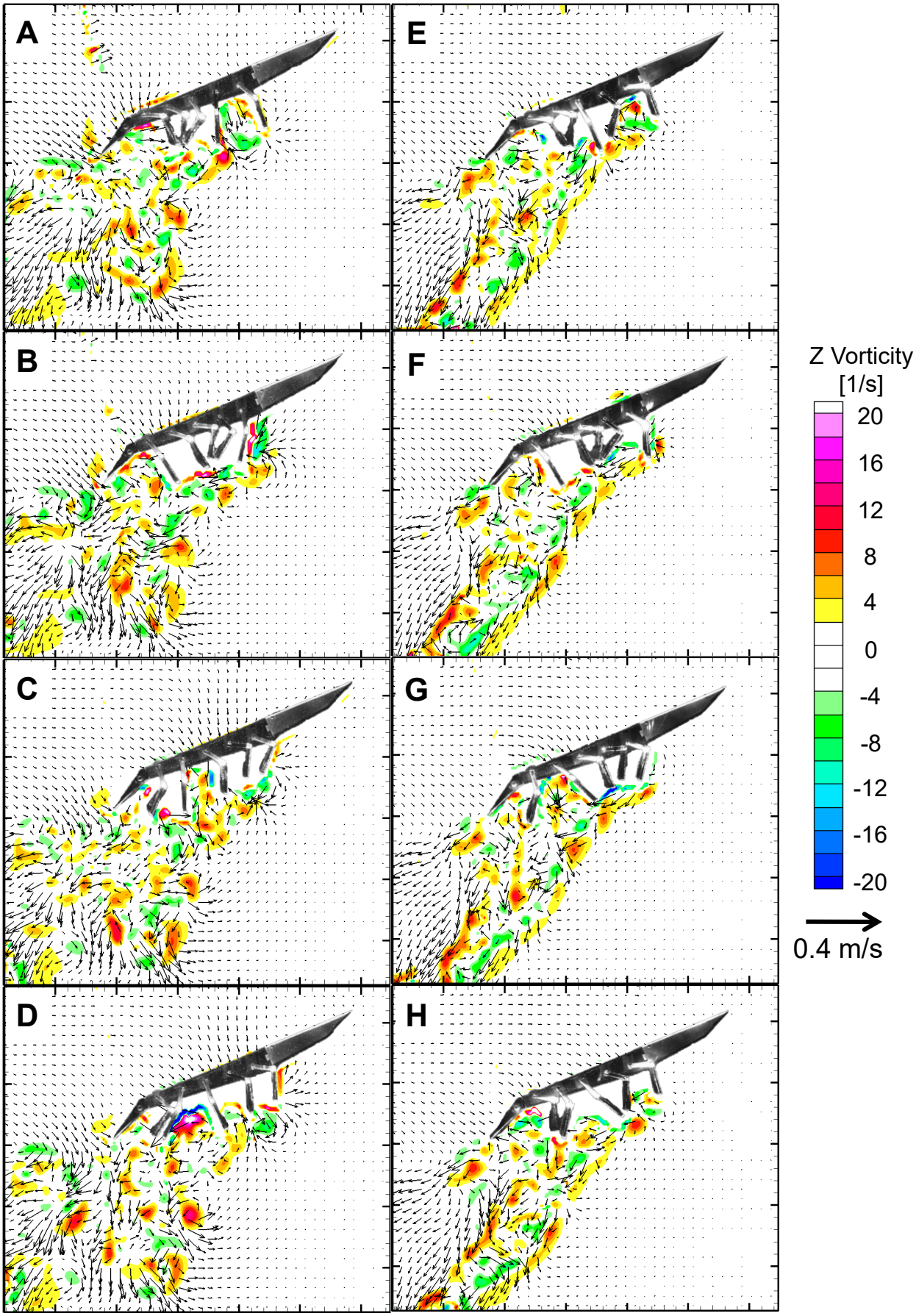

Figure 5

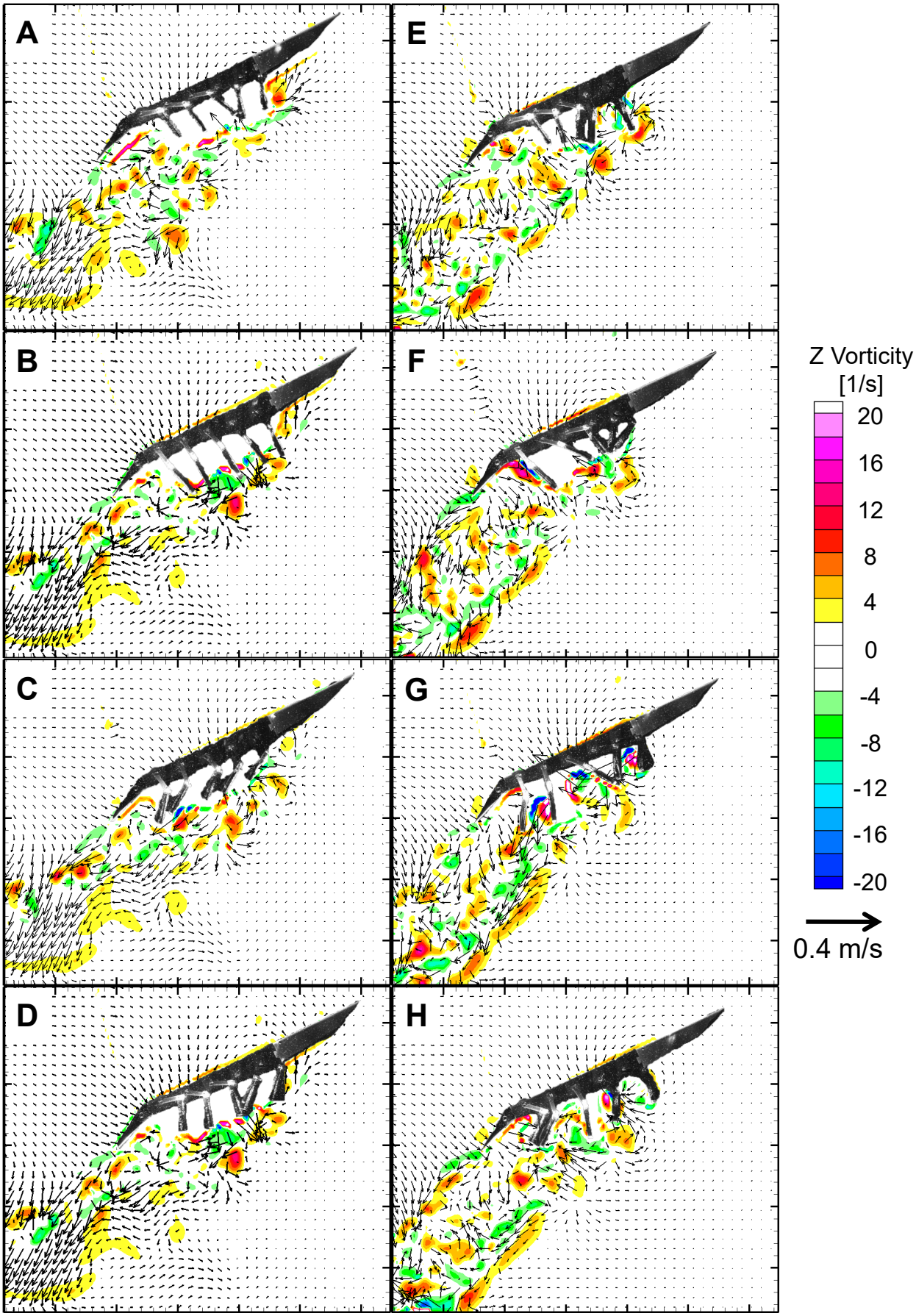

Figure 6

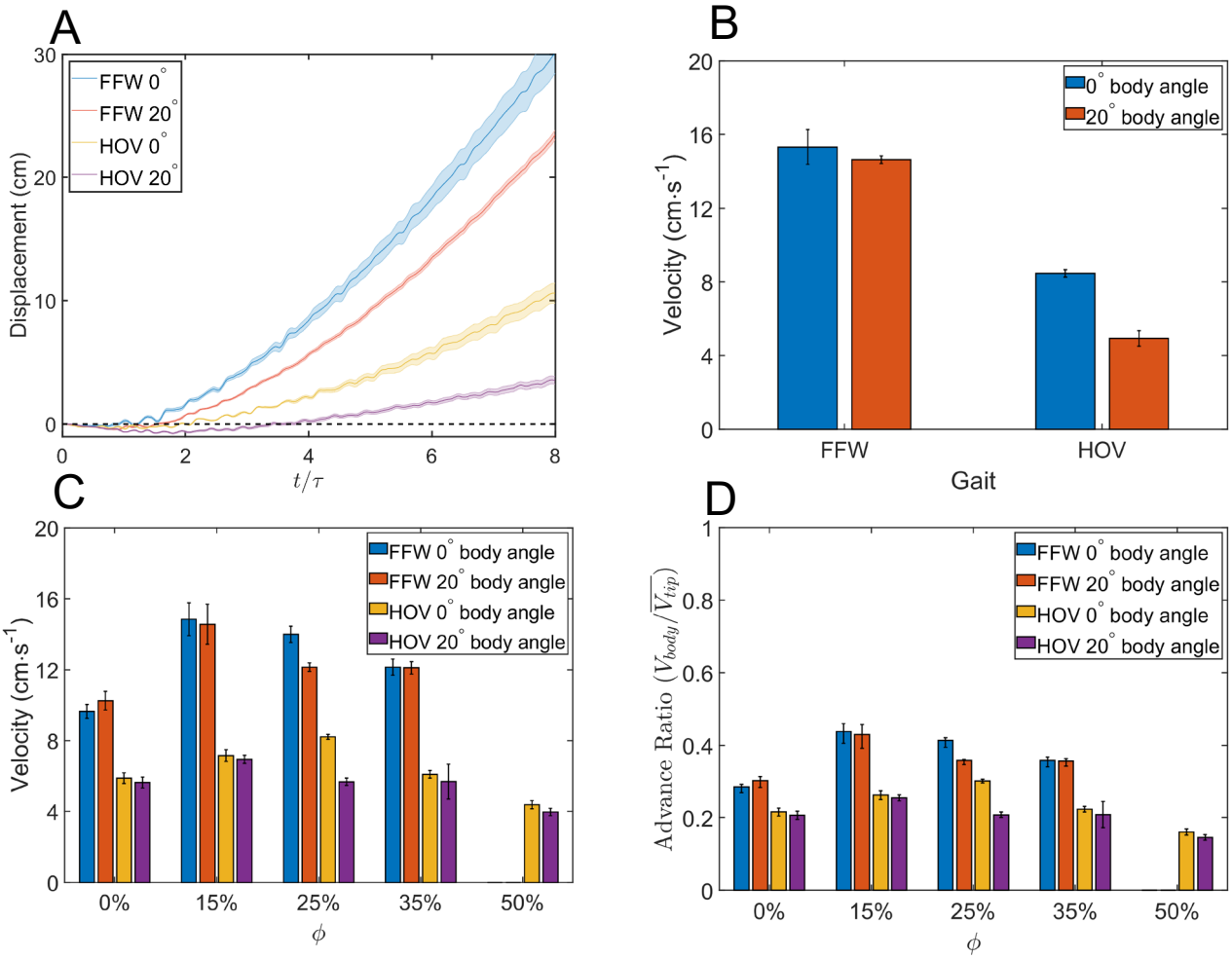
A
FFW 0°
FFW 20°
HOV 0°
HOV 20°
Displacement (cm)
t/τ
B
0° body angle
20° body angle
Velocity (cm·s^{-1})
FFW
HOV
Gait
C
FFW 0° body angle
FFW 20° body angle
HOV 0° body angle
HOV 20° body angle
Velocity (cm·s^{-1})
0%
15%
25%
35%
50%
ϕ
D
FFW 0° body angle
FFW 20° body angle
HOV 0° body angle
HOV 20° body angle
Advance Ratio ($V_{body}/\overline{V_{tip}}$)
0%
15%
25%
35%
50%
ϕ

Figure 7

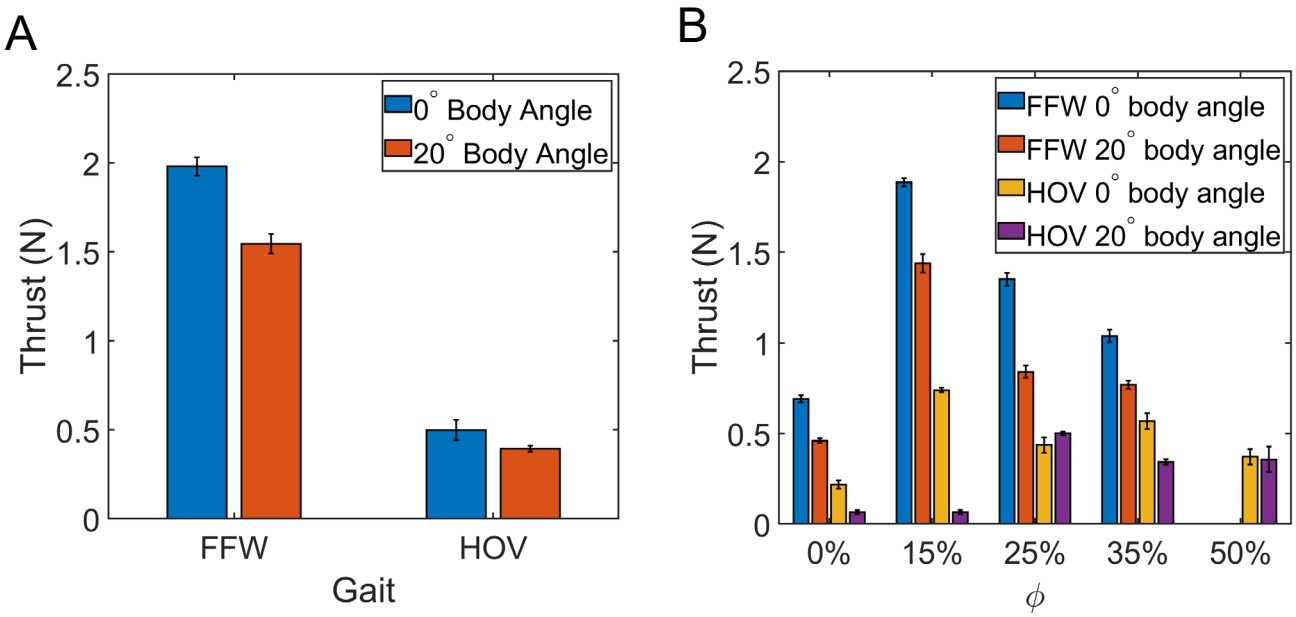
A
2.5
2
1.5
1
0.5
0
Thrust (N)
0° Body Angle
20° Body Angle
FFW
HOV
Gait
B
2.5
2
1.5
1
0.5
0
Thrust (N)
FFW 0° body angle
FFW 20° body angle
HOV 0° body angle
HOV 20° body angle
0%
15%
25%
35%
50%
ϕ

Figure 8

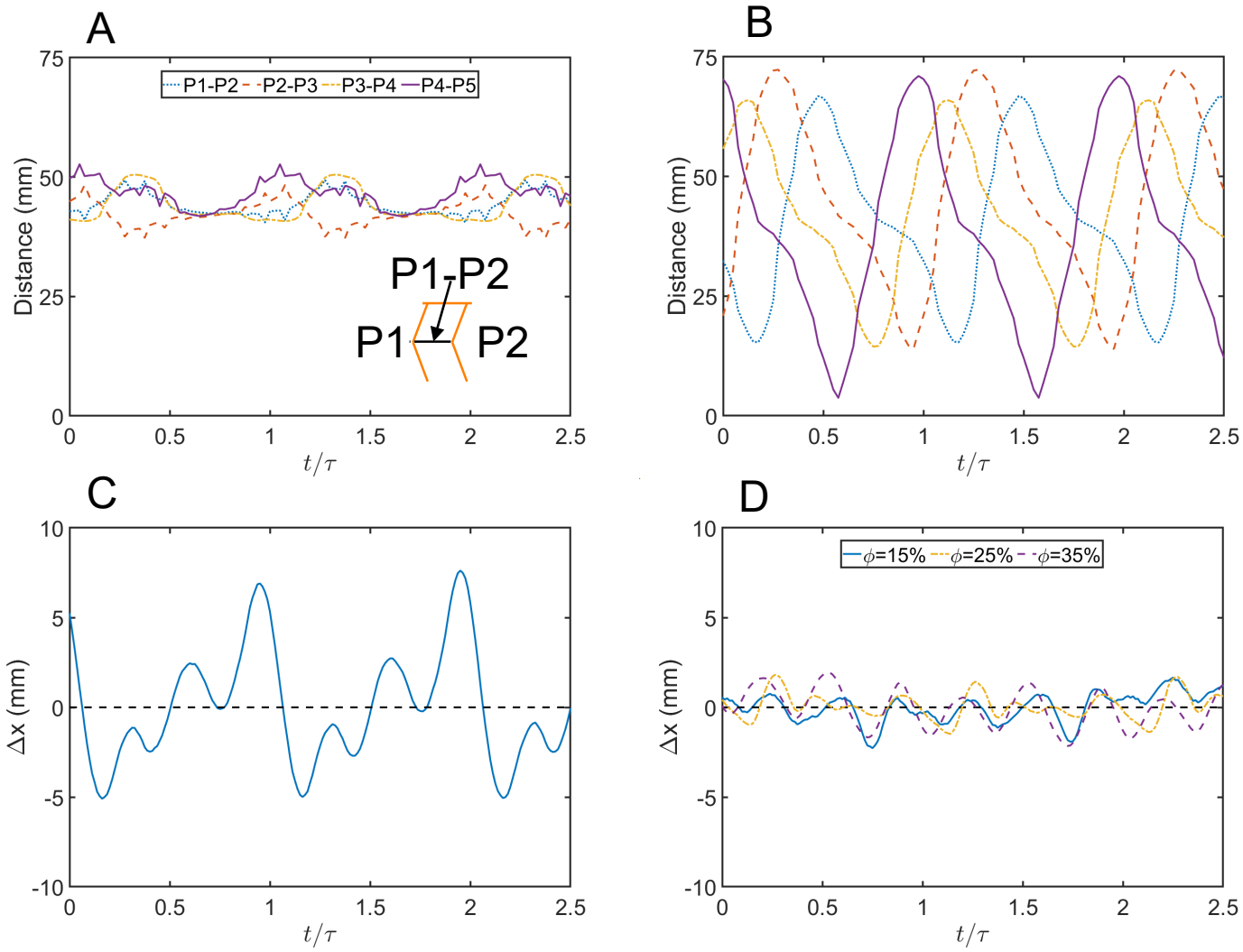
A
B
C
D
P1-P2
P2-P3
P3-P4
P4-P5
P1-P2
P1
P2
Distance (mm)
Δx (mm)
t/τ
ϕ=15%
ϕ=25%
ϕ=35%